DUAL-TIME-POINT PATLAK ESTIMATION FROM LIST MODE PET DATA

*†Wentao Zhu, *Quanzheng Li, †Richard M. Leahy*

†Signal and Image Processing Institute, University of Southern California, Los Angeles, CA 90089
*Department of Radiology, Massachusetts General Hospital, Boston, MA, 02114

ABSTRACT

We investigate the potential of using dual-time-point PET data to perform Patlak modeling. If successful this approach could be used for whole-body dynamic PET in which we compute voxel-wise estimates of Patlak parameters using two frames of data for each bed position. Our approach directly uses list-mode arrival time for each event to compute the Patlak image. We evaluate performance of the method in comparison to fractional changes in SUV values computed from the same two frames of data. The area under ROC curves is used as a figure of merit to assess the relative performance of these two approaches in differentiating tumor from background. We calculate ROC curves using (i) variance estimates computed from the Cramer-Rao bound for a simplified 1D version of the problem and (ii) 4D Monte Carlo simulations of tumors with a range of sizes in a uniform background. Both the simulation and Cramer-Rao analysis suggest that our dual-time-point Patlak estimation method can achieve superior differentiation of tumor from background in small tumors compared to using fractional changes in SUV computed from the same dual-time-point data.

Index Terms— Patlak, dynamic PET, lesion detection

1. INTRODUCTION

To accommodate the full length of a patient, whole-body PET studies are collected in several frames, one at each of multiple bed positions. Since dynamic PET methods typically require continuous acquisition they have not been used in whole-body studies. Here we explore the potential for dynamic imaging from multiframe data of the type that can be acquired in a whole body scanning protocol.

The standardized uptake value (SUV) is computed as the mean uptake in a single frame in a region of interest normalized by dose and patient weight. This semi-quantitative measure is used in cancer staging and in following response to therapy. The impact of SUV as a biomarker is limited by its use of a single frame of data so that it does not reflect the underlying dynamics of tracer uptake. Variations in protocols among clinical sites and the complex relationship between dose, uptake and body weight further limits its use as a quantitative biomarker. Masa-Ah et al. [1] also found that SUV values correlate with factors such as dose extravasations, attenuation parameters, partial volume effect, and plasma glucose level in blood as well as iterative updates in reconstruction. Wiyaporn et al. [2] showed that SUV values increase with the number of OSEM iterations and are also affected by tumor size.

To overcome some of these limitations several researchers have investigated the use of two or more frames of data at each body position. Alkhawaldeh et al. [3] found that dual-time-point PET can improve diagnostic accuracy relative to standard single frame SUV, increasing sensitivity and specificity for malignant lung nodules, especially for small lung lesions that have low SUVs. Prieto et al. [4] showed that dual-time-point PET can improve sensitivity for the identification and volume delineation of high-grade brain tumors compared with standard PET studies. Imbriaco et al. [5] investigated a group of patients with suspected breast malignancy and found higher accuracy and sensitivity than single-time-point PET. Hu et al. [6] reported similar conclusions for mediastinal nodal staging, finding that specificity, accuracy, and positive predictive value of dual-time-point scans were better than those of single-time-point.

Typically the above studies look at fractional changes in SUV (%DSUV) from one time frame to the next. Here we investigate the question of whether Patlak parameters extracted from the same data may provide better differentiation between tissues with differential uptake than do %DSUV values.

2. METHOD

2.1 Patlak Estimation from two Frame List Mode Data: The Patlak graphical model applies to kinetic data beyond time $t \geq T^*$ at which changes are effectively due to irreversible trapping in a single compartment. Let $\eta(t)$ be the tracer time activity curve (TAC) with input function $C(t)$. We can write the Patlak equation [2] as:

$$\eta(t) = \kappa \int_0^t C(\tau)d\tau + qC(t)$$

where κ is the net influx rate, and q is the intercept of the Patlak model. We can therefore model the rate function at voxel j after steady state $t \geq T^*$ as a linear combination of two basis functions:

$$\eta_j(t) = \sum_{l=1}^{2} \omega_{jl} B_l(t)$$

$$\omega_{j1} = \kappa_j, \omega_{j2} = q_j, B_1(t) = \int_0^t C(\tau)d\tau\,, B_2(t) = C(t)$$

Consequently the rate function in sinogram space at line of response (LOR) *i* can be written as:

$$\lambda_i(t) = e^{-t/\tau} \sum_{j=1}^{n_v} \sum_{l=1}^{2} p_{ij} \omega_{jl} B_l(t)$$

where the exponential term accounts for radioactive decay of the tracer, and p_{ij} is the probability of an event at voxel *j* being detected at detector pair *i*.

Assuming we have continuous list mode data over the interval $[T^*, T]$ and the arrival times in the list mode data follow an inhomogeneous Poisson model, then the continuous time log-likelihood function of event arrival times is given by:

$$L(W) = -\sum_{i=1}^{n_p} \sum_{k=1}^{x_i} log\lambda_i(a_{ik}) + \sum_{i=1}^{n_p} \int_{T^*}^{T} \lambda_i(t)dt$$

where a_{ik} denotes the arrival time of the *k*'th photon at detector pair *i*, x_i is the number of events detected in LOR *i,* and n_p is the total number of LORs. In the case where we collect data only over two subintervals $[t_1, t_2]$ and $[t_3, t_4]$, the log likelihood is modified as follows:

$$L(W) = -\sum_{i=1}^{n_p} \sum_{k=1}^{x_i} log\lambda_i(a_{ik}) + \sum_{i=1}^{n_p} \left(\int_{t_1}^{t_2} \lambda_i(t)dt + \int_{t_3}^{t_4} \lambda_i(t)dt \right)$$

where the a_{ik} are constrained to events detected only in the interval $[t_1\ t_2]$ or $[t_3\ t_4]$. We use $L(W)$ as a cost function from which we compute a maximum likelihood estimate of the Patlak parameters at each voxel. As we have described earlier [7], optimization can be performed using a 4D incremental gradient method [8].

2.2 The Cramer-Rao Lower Bound (CRLB): we can use the CRLB computed from the log likelihood function to explore lower bounds on the performance of this technique. The bounds are found from the inverse of the Fisher information matrix (FIM) defined as

$$F_{mj,nl} = -E\left[\frac{\partial L^2(W)}{\partial \omega_{mj} \partial \omega_{nl}}\right]$$

Where each element in this matrix of second order derivatives is given by:

$$\frac{\partial L^2(W)}{\partial \omega_{mj} \partial \omega_{nl}} = \sum_{i=1}^{n_p} \sum_{k=1}^{x_i} \left\{ \frac{e^{-\frac{2a_{ik}}{\tau}} p_{im} p_{in} B_j(a_{ik}) B_l(a_{ik})}{{\lambda_i}^2(a_{ik})} \right\}$$

To find the FIM we need to integrate this matrix over the probability density function for the arrival time a_{ik} for each photon: $\sum_{p_1=1}^{\infty} \sum_{p_2=1}^{\infty} f_k(a_{ik}|p_1, p_2)\ P(p_1)\ P(p_2)$ where

$$f_k(a_{ik}|p_1, p_2) = \begin{cases} \dfrac{\lambda_i(a_{ik}) \dfrac{\left(\int_{t_1}^{t_k} \lambda_i(\tau)\, d\tau\right)^{k-1}}{(k-1)!} \dfrac{\left(\int_{t_k}^{t_2} \lambda_i(\tau)\, d\tau\right)^{p_1-k}}{(p_1-k)!}}{e^{\int_{t_1}^{t_2} \lambda_i(\tau)d\tau} P(p_1)} & k \le p_1 \\ \dfrac{\lambda_i(a_{ik}) \dfrac{\left(\int_{t_3}^{t_k} \lambda_i(\tau)d\tau\right)^{k-p_1-1}}{(k-p_1-1)!} \dfrac{\left(\int_{t_k}^{t_4} \lambda_i(\tau)d\tau\right)^{p_2+p_1-k}}{(p_2+p_1-k)!}}{e^{\int_{t_3}^{t_4} \lambda_i(\tau)d\tau} P(p_2)} & k > p_1 \end{cases}$$

under the condition that there are p_1 arrivals in first frame time $[t_1\ t_2]$ and p_2 arrivals in the second frame $[t_3\ t_4]$ with respective probabilities $P(p_1)$ and $P(p_2)$.

3. RESULTS

3.1 Cramer-Rao Analysis: since the difference between %DSUV and Patlak analysis lies largely in the handling of the dynamic rather than the spatial information, we can obtain insight into the problem through consideration of a simplified 1D problem corresponding to a single image voxel from which we directly observe Poisson counts generated according to the dynamic TAC $\eta(t)$. We computed CRLBs for the Patlak slope parameter and %DSUV for this 1D problem from a two compartmental model with parameters chosen to reflect (a) tumor dynamics, (b) normal tissue dynamics. Assuming the Patlak parameter estimator is unbiased and approximately Gaussian we can determine the distribution of Patlak values for cases (a) and (b). The ROC curve for detection of tumor vs. background can then be determined directly from these distributions. Similarly, we assume that SUV values are Gaussian with a variance equal to the mean number of counts in each frame. The %DSUV will then have a distribution formed by a ratio of Gaussians, and again we can compute the ROC curve for cases (a) and (b). An example of the distributions obtained for the two cases with the parameter values listed in Table 1 is shown in Fig. 1, with corresponding ROC curves in Fig. 2. These examples correspond to relatively low count scenarios; however over a full range of count rates we find that the area under the ROC curve for the Patlak method is consistently higher than

that for the %DSUV. With this result we then proceeded to a larger scale study using 3D PET data which is more readily investigated by Monte Carlo simulation.

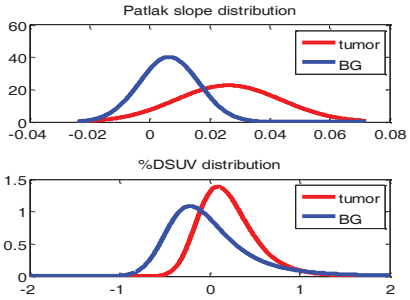


Fig. 1. Distribution of Patlak (upper) and %DSUV (lower) values for tumor and background (BG).

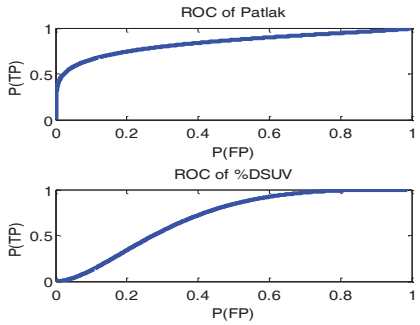


Fig. 2. Cramer-Rao based ROC curves for patlak (upper) and %DSUV (lower).

Region	K1 ml/min/g	k2 ml/min/g	k3 ml/min/g	k4 ml/min/g
BG	0.5333	0.9800	0.0120	0
Tumor	0.1980	0.2280	0.0350	0

Table 1. kinetic parameters used for background and tumor

3.2 Data Simulation: For these studies we simulated a small scale 3D PET system (diameter: 148.4mm, detector size: 2.423mm×2.423mm; number of rings: 4) with a total of 13 sinograms with 84 angles of view by 96 radial lines of response (LORs). A uniform cylindrical phantom of diameter 31.4mm was centered in the scanner and contained 5 cylinders ("tumors") of diameter 1.0, 1.8, 2.6, 3.4, and 4.2mm as shown in Fig. 3. We simulated time activity curves for tumors and background using the parameters in Table 1 and the blood input function shown in Fig. 4. The time activity curves (TACs) for each sinogram element were computed by forward projection through a system matrix generated for the scanner described above. Each of these TACs represents the mean of the data for each LOR at each point in time. The TACs were then treated as the rate function of an inhomogeneous Poisson process from which we generated pseudorandom list mode events (LOR and arrival times). In the results presented here we then windowed the data to retain only those events corresponding to two five minute frames starting at 40min and 80min. We generated a total of 100 Monte Carlo trials, each with the same phantom.

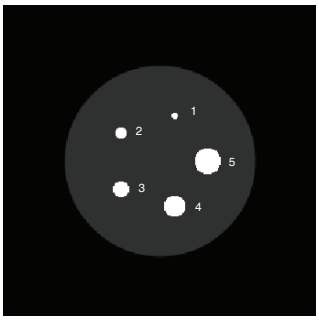


Fig. 3. Uniform cylinder ("background") with 5 cylinders ("tumor") of different sizes.

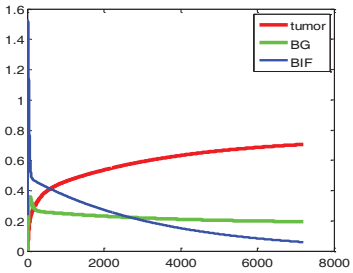


Fig. 4. Simulated time-activity-curves for tumor, background and the blood input function.

3.3 Patlak Estimation: We used the modified 4D incremental gradient (4DIG) algorithm [7] to reconstruct images of Patlak slope and intercept. For each of the 100 trials we computed the average slope parameter for each of 5 tumor ROIs and 5 corresponding background ROIs with sizes chosen to match those of the tumor ROIs. By comparing the means and s.d. of tumor ROIs to matched background ROIs we computed ROC curves for the differentiability of the tumor relative to background as a function of lesion size. The mean of the Patlak slope images over the 100 trials is shown in Fig. 5 and the mean and s.d. for each ROI is listed in Table 2. The areas under the ROC curves are in Table 3.

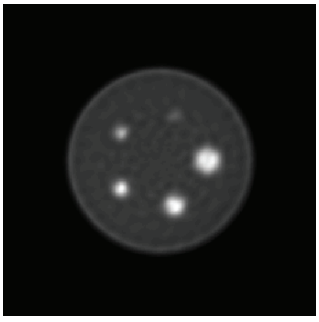


Fig. 5. One transaxial slice of the mean of the estimated Patlak slope images estimated from two frame list mode data for each of the 100 Monte Carlo trials.

	Patlak		%DSUV	
ROI	Tumor	BG	Tumor	BG
1	0.0106±8.35 e-4	0.0064±6.51 e-4	0.0809±0.1300	- 0.0935±0.1400
2	0.0190±9.58 e-4	0.0065±4.73 e-4	0.1513±0.0720	- 0.0904±0.0926
3	0.0229±7.77 e-4	0.0065±3.87 e-4	0.1527±0.0380	- 0.0881±0.0624
4	0.0262±5.22 e-4	0.0064±2.93 e-4	0.1539±0.0265	- 0.0898±0.0425
5	0.0264±4.59 e-4	0.0065±2.30 e-4	0.1570±0.0216	- 0.0901±0.0338
True value	0.0263	0.0065	0.1640	- 0.0903

Table 2. Mean and standard deviation of estimated Patlak slope and %DSUV values for 5 tumor regions v.s. BG regions of the same size

3.4 %DSUV Calculation: We used the same two frame data to reconstruct two static PET images using MAP estimation. To make a fair comparison, we adjusted the smoothing parameters so that the resolution of the static reconstructed image approximately matched that of the Patlak slope image. We then calculated the SUV values for each of the ROIs for both frames and %DSUV = (SUV2-SUV1)/SUV1. Repeating the process for the 100 trials we then computed mean and s.d. of %DSUV for each ROI, listed in Table 2. As with the Patlak images, we then use these statistics to compute ROC curves and the area under each curve, as listed in Table 3.

ROC area	Tumor 1 vs BG1	Tumor 2 vs BG2	Tumor 3 vs BG3
Patlak	0.9998	1.00	1.00
%DSUV	0.8471	0.9781	1.00

Table 3. ROC areas of Patlak and %DSUV for 5 tumor regions v.s. BG regions of the same size

4. DISCUSSION AND CONCLUSION

Our results indicate that for the two smaller tumors, the areas under the ROC curve are lower for percentage SUV than for Patlak estimation. For the larger tumors, both show perfect detection results (unit area under the ROC curve). These results are dependent on the specific choice of rate parameters and count rate, however so far we have seen performance consistent with that reported above when we varied these parameters. The Cramer-Rao analysis reveals similar behavior, albeit in a simplified setting. The advantage of the Cramer-Rao approach is that we can explore a much wider range of parameters than in a full scale 4D Monte Carlo simulation. We can therefore use the Monte Carlo results to guide parameter selection (e.g. start and end times for each of the frames) prior to performing more realistic Monte Carlo studies. In both the simulations and Monte Carlo studies we have attempted to perform a fair comparison in the sense that Patlak and percentage SUV values are both estimated from the same underlying dynamic processes. Consequently, while these first simulations are relatively simple, these results provide encouraging support for exploring performance of dual-time-point Patlak analysis, relative to fractional SUV, in more realistic simulations and real experimental and clinical data.

Acknowledgement: this work is supported by NIH grants R21CA149587, R01EB013293, and R01EB010197.

5. REFERENCES

[1] P. Masa-Ah, M. Tuntawiroon, S. Soongsathitanon, "A novel scheme for Standardized Uptake Value (SUV) calculation in PET scans, " *international journal of mathematical models and methods in applied sciences*, vol 4(4), pp: 291-299, 2010

[2] K. Wiyaporn, C. Tocharoenchai, P. Pusuwan, T. Ekjeen, S. Leaungwutiwong, S. Thanyarak, "Factors Affecting Standardized Uptake Value (SUV) of Positron Emission Tomography (PET) Imaging with 18F-FDG, " *J Med Assoc Thai*, vol. 93(1), pp: 108-114, 2010

[3] K. Alkhawaldeh, G. Bural, R. Kumar, A. Alavi, "Impact of dual-time-point 18F-FDG PET imaging and partial volume correction in the assessment of solitary pulmonary nodules, " *Eur J Nucl Med Mol Imaging*, vol 35, pp: 246–252, 2008

[4] E. Prieto, JM. Martí-Climent, I. Domínguez-Prado, P. Garrastachu , R. Díez-Valle, S. Tejada, JJ. Aristu, I. Peñuelas, J. Arbizu, "Voxel-based analysis of dual-time-point 18F-FDG PET images for brain tumor identification and delineation, " *J Nucl Med*, vol 52(6), pp: 865-872, Jun 2011

[5] M. Imbriaco, M.G. Caprio, G. Limite, L. Pace, T.D. Falco, E. Capuano, M. Salvatore, "Dual-time-point 18F-FDG PET/CT versus dynamic breast MRI of suspicious breast lesions, " *Ajr American Journal Of Roentgenology*, vol 191(5), pp: 1323-1330, 2008

[6] M. Hu, A. Han, L. Xing, W. Yang, Z. Fu, C. Huang, P. Zhang, L. Kong, J. Yu, "Value of dual-time-point FDG PET/CT for mediastinal nodal staging in non-small-cell lung cancer patients with lung comorbidity, " *Clin Nucl Med*, vol 36(6), pp: 429-433, Jun 2011

[7] Q. Li and R.M. Leahy, "Direct Estimation of Patlak Parameters from List Mode PET Data, " *in Proc. ISBI*, pp.390-393, 2009

[8] Q Li, E Asma, S Ahn, RM Leahy, "A Fast Fully 4D Incremental Gradient Reconstruction Algorithm for List Mode PET Data, " *IEEE Trans. Med. Imag*, 26 (1):58-67, 2007